# Catalysis Science & Technology

Accepted Manuscript






ROYAL SOCIETY OF CHEMISTRY

www.rsc.org/catalysis

Catalysis Science & Technology

ARTICLE

# Selective dehydrogenation of bioethanol to acetaldehyde over basic USY zeolites

Received 00th January 20xx,
Accepted 00th January 20xx

DOI: 10.1039/x0xx00000x

www.rsc.org/

G. M. Lari, K. Desai, C. Mondelli and J. Pérez-Ramírez*

Zeolites featuring basic sites have displayed outstanding performance in the valorisation of biobased substrates through condensation and coupling reactions. Herein, we present the continuous-flow, gas-phase dehydrogenation of ethanol to acetaldehyde as a novel application of recently developed alkali-activated high-silica USY zeolites. Evaluation of the hydroxides of Group 1 metals in the catalyst preparation by alkaline treatment identified sodium hydroxide as the most suited base. This is due to the stronger character and the higher number of mild basic sites formed coupled to the minimal impact on the pristine porous properties of the zeolite, which resulted in superior catalytic performance. Compared to existing basic catalysts such as MgO and hydroxyapatites, no $C_4$-condensation products were observed and the occurrence of ethanol dehydration to ethylene was marginal owing to the negligible acidity of the material. At the optimal reaction temperature, acetaldehyde was attained with a *ca.* 15-fold higher yield (50%) and with high selectivity (80%) adding oxygen to the ethanol feed. The origin of this peculiar positive behaviour was unraveled through kinetic and *in situ* infrared spectroscopic studies as well as by temperature-programmed surface reaction of ethanol. These investigations revealed the exclusive presence of ethoxide species at the catalyst surface, which (*i*) are formed upon adsorption of ethanol at basic siloxy groups, (*ii*) are stabilised through hydrogen bonding with vicinal silanols and (*iii*) react in a rate-limiting step with gas-phase oxygen through an Eley-Rideal mechanism to form acetaldehyde releasing water. The stable performance of the material over 24 h on stream strongly contrasts with the rapid activity decline of noble metal-based catalysts studied for this transformation.

## Introduction

Light aldehydes are important chemical intermediates. Thanks to the high reactivity of their carbonyl group, they can be transformed into multiple products through oxidation and (poly)condensation.[1] The routes currently practiced for their preparation include hydroformylation[2] and oxidation[3] of alkenes, but dehydrogenation of alcohols could attract a strong interest in the near future in view of the possibility to easily attain these substrates from renewable feedstocks.[4] So far, bulk and supported catalysts based on palladium[5], silver[6] and, especially, copper[7] and gold[8] have been shown to selectively catalyse the dehydrogenation of ethanol to acetaldehyde but they are characterised by low turnover frequencies and fast deactivation due to sintering.[7-9] Still, Veba-Chemie commercialised a process based on elementary silver, which has been quite widely applied till the 1990s.[6c] Attempts to increase stability by addition of modifiers, chiefly chromium, have led to only moderate improvements.[9] Reducible transition-metal oxides such as $Mn_xO_y$ have been found structurally more robust but produced greater amounts of ethyl acetate than acetaldehyde over the same sites active for dehydrogenation at high conversion levels.[10] Materials containing basic centres, which catalyse dehydrogenation owing to their proton abstraction ability,[11] could comprise an appealing alternative. In this respect, MgO was proved able to dehydrogenate methanol and ethanol.[12] Still, poor selectivity to the aldehyde was observed due to its fast subsequent transformation into 1,3-butadiene through condensation.[13] Intermolecular secondary reactions have been suppressed using high-surface area basic MFI zeolites obtained by impregnation of silicalite with sodium salts, which feature a lower density of active sites.[14] However, these materials by-produced ethylene due to residual acidity. Harsh heat treatments were successful in removing the latter but lead to lower reaction rates due to partial amorphisation of the framework.

Recently, high-silica Na-containing ultra-stable Y (USY) zeolites were demonstrated as active base catalysts for Knoevenagel and (nitro)aldol condensations.[15] An increase of their basic character and, in turn, of their performance was obtained by alkaline treatment of these materials.[16] In this case, the catalytic centres were identified as siloxy groups obtained through exposure of silanols to the sodium hydroxide solution.

*Institute for Chemical and Bioengineering, Department of Chemistry and Applied Biosciences, ETH Zurich, Vladimir-Prelog-Weg 1, CH-8093 Zurich, Switzerland.*
*E-mail: jpr@chem.ethz.ch; Fax: +41 44 6331405; Tel: +41 44 6337120*

Electronic Supplementary Information (ESI) available: calibration curve for the GC analysis of ethanol, characterisation data by FTIR spectroscopy of adsorbed pyridine of MgO, Ca-HAP, USY and NaUSY-01 and by $CO_2$-TPD of MgO and Ca-HAP and equilibrium conversion curves simulated with Aspen for ethanol dehydration and dehydrogenation with the calculation details. See DOI: 10.1039/x0xx00000x

Lately, the post-synthetic modification was shown to be better performed using methanol as the solvent instead of water in order to better retain the porous and structural properties of the starting zeolite.[17] Indeed, treatment of high-silica faujasites in aqueous NaOH introduced beneficial mesoporosity but led to a significant decrease in the crystallinity.

Herein, we apply high-silica basic USY zeolites for the selective dehydrogenation of ethanol to acetaldehyde. We study the impact of the nature and concentration of the alkali hydroxide employed in their preparation on the catalytic properties of the materials. Thereafter, we optimise the performance of the best catalyst adjusting the reaction conditions and adding oxygen to the feed and evaluate the stability of the system. Finally, we conduct kinetic, *in situ* infrared spectroscopic and temperature-programmed surface reaction studies to gather insights into the mechanism of the transformation.

## Experimental

### Catalyst preparation

Alkaline-activation of USY (Si/Al = 405, Tosoh Corporation) was performed adding 3.3 g of zeolite to 100 $cm^3$ of a 0-0.3 M methanolic (Sigma-Aldrich, 99.8%) solution of NaOH (Sigma-Aldrich, 97%), KOH (Fisher Chemicals, 85%), $RbOH{\cdot}2H_2O$ (Fluka, 95%) or CsOH (50 wt.% $CsOH/H_2O$, ABCR, 99.9%). After stirring for 10 min at room temperature, the solid was filtered, washed with the same solvent used for the treatment (3 times, *ca.* 100 $cm^3$ each time) and dried at 338 K for 16 h. The samples obtained were denoted as MUSY-0.*x*, where M indicates the cation introduced in the material depending on the nature of the base and 0.*x* the concentration of the base. The yield of the treatment ($Y_{treat}$) was calculated as

$$Y_{treat} = m_{cat} / (m_{parent} + 0.1\ L \cdot C_{MOH} \cdot AW_M)$$

where $m_{cat}$ is the mass of the dry material after synthesis, $m_{parent}$ is the mass of the parent zeolite, $C_{MOH}$ is the concentration of the hydroxide used in the preparation and $AW_M$ the atomic weight of the alkali cation in the base. MgO (Strem chemicals, 99.5%) and calcium hydroxyapatite (Ca-HAP, Acros Organics) were used as benchmark catalysts after drying at 338 K for 16 h.

### Catalyst characterisation

The Na and Si contents in the samples were determined by inductively coupled plasma optical emission spectroscopy (ICP-OES) using a Horiba Ultra 2 instrument equipped with a photomultiplier tube detector. The K, Rb and Cs contents were measured by X-ray fluorescence (XRF) using an EDAX Orbis Micro-XRF analyser equipped with an Rh source operated at a voltage of 30 kV and a current of 500 μA. Powder X-ray diffraction (XRD) was performed using a PANalytical X'Pert PRO-MPD diffractometer with Ni-filtered Cu K$\alpha$ radiation ($\lambda$ = 0.1541 nm), acquiring data in the 5-70° 2$\theta$ range with a step size of 0.05° and a counting time of 8 s per step. $N_2$ sorption at 77 K was conducted using a Micromeritics TriStar analyser. Prior to the measurements, the samples were degassed at 573 K under vacuum for 3 h. Temperature-programmed desorption of carbon dioxide ($CO_2$-TPD) and temperature-programmed surface reaction of ethanol (EtOH-TPSR) were carried out using a Micromeritics Autochem II chemisorption analyser coupled with a MKS Cirrus 2 quadrupole mass spectrometer. For $CO_2$-TPD, the catalyst (0.05 g) was pre-treated in He flow (20 $cm^3$ $min^{-1}$) at 823 K for 2 h. Afterwards, $CO_2$ (50 pulses, 1 $cm^3$) diluted in He flow (10 $cm^3$ $min^{-1}$) was adsorbed at 323 K, followed by He purging at the same temperature for 1 h. $CO_2$ desorption was monitored in the range of 323-973 K using a heating rate of 10 K $min^{-1}$. The $C_{base}/C_M$ parameter was obtained as the fraction between the area of the integrated $CO_2$-TPD curve and the fraction of alkali metal in the solid (M/(M+Si)). In the case of EtOH-TPSR, the catalyst (0.05 g) was pre-treated in He flow (20 $cm^3$ $min^{-1}$) at 673 K for 2 h. Afterwards, 50 pulses (1 $cm^3$) of EtOH-saturated He were adsorbed at 323 K, followed by He purging at 373 K for 1 h. The evolution of the products was monitored in the range of 323-973 K at 10 K $min^{-1}$. Fourier transform infrared (FTIR) spectroscopy of adsorbed pyridine was conducted using a Bruker IFS66 spectrometer equipped with an MCT detector. Wafers (*ca.* 1 $cm^2$, 20 mg) were degassed at 693 K under vacuum for 4 h, cooled to room temperature and exposed to pyridine vapours (Sigma-Aldrich, >99%). Thereafter, they were evacuated at room temperature (15 min) and 473 K (30 min). Spectra were recorded in the 4000-1300 $cm^{-1}$ range by accumulation of 32 scans with a resolution of 4 $cm^{-1}$. The concentration of Brønsted- and Lewis-acid sites was determined by integration of the peaks at 1545 and 1455 $cm^{-1}$ using 1.67 and 2.22 cm μmol$^{-1}$ as the extinction coefficients, respectively. Diffuse-reflectance Fourier transform infrared (DRIFT) spectroscopy was performed using a Bruker Optics Vertex 70 spectrometer equipped with a high-temperature DRIFT cell (Harrick) and an MCT detector. Spectra were recorded in the range of 4000-400 $cm^{-1}$ at 723 K under a flow of 4 vol.% ethanol (EtOH)/2 vol.% $O_2$/He or 4 vol.% EtOH/He by co-addition of 200 scans with a resolution of 4 $cm^{-1}$. Prior to the measurements, the samples were dried at 673 K under He flow for 4 h. Transmission electron microscopy (TEM) and high-angle annular dark field scanning transmission electron microscopy (HAADF-STEM) images and energy dispersive X-ray spectroscopy (EDS) element maps were acquired using a FEI Talos instrument operated at 200 kV. Powdered samples were deposited on Mo-grids. HAADF images were collected before and after EDS measurements to corroborate the absence of morphological changes.

### Catalytic testing

Catalytic tests were performed in an Effi Microactivity reactor (PID Eng&Tech) equipped with (*i*) mass flow controllers to feed $N_2$ (PanGas, 99.995%) and 20 vol.% $O_2/N_2$ (PanGas), (*ii*) an HPLC pump to feed EtOH (Sigma-Aldrich, 99.5%), (*iii*) a reactor (i.d. = 9 mm) heated in an oven and contained in a hot box and (*iv*) an on-line gas-chromatograph (GC, Agilent 5890) equipped with a HP-5 column. To avoid condensation of the outlet gases before the analysis, the hot box and the line connecting the reactor to the GC were heated at 423 K. The reactor was



 

**Table 1.** Characterisation data of the alkali-containing USY zeolites.

| Catalyst | $Y_{treat}$ (%) | M[a] (wt. %) | Metallation efficiency (%)[b] | $V_{pore}$[c] ($cm^3\ g^{-1}$) | $V_{micro}$[d] ($cm^3\ g^{-1}$) | $S_{meso}$[d] ($m^2\ g^{-1}$) | $S_{BET}$[e] ($m^2\ g^{-1}$) | $C_{basic\ sites}$[f] (a.u.) | $C_{basic\ sites}$ / $C_M$[g] (a.u.) |
|---|---|---|---|---|---|---|---|---|---|
| USY | - | 0.09 | - | 0.53 | 0.29 | 100 | 648 | 0.0 | 0.0 |
| NaUSY-0.025 | 93.8 | 0.54 | 31 | 0.53 | 0.29 | 104 | 660 | 6.3 | 4.5 |
| NaUSY-0.05 | 90.8 | 0.67 | 19 | 0.53 | 0.28 | 100 | 640 | 9.0 | 5.1 |
| NaUSY-0.1 | 84.1 | 1.05 | 15 | 0.49 | 0.25 | 86 | 600 | 37.8 | 13.8 |
| NaUSY-0.2 | 75.5 | 2.46 | 18 | 0.42 | 0.23 | 72 | 515 | 29.5 | 4.6 |
| NaUSY-0.3 | 66.9 | 2.80 | 13 | 0.36 | 0.19 | 64 | 463 | 11.7 | 1.6 |
| KUSY-0.1 | 87.0 | 4.08 | 36 | 0.42 | 0.21 | 43 | 462 | 30.7 | 4.7 |
| RbUSY-0.1 | 78.7 | 11.2 | 49 | 0.43 | 0.22 | 53 | 492 | 23.0 | 2.6 |
| CsUSY-0.1 | 77.3 | 16.3 | 56 | 0.35 | 0.20 | 35 | 425 | 19.2 | 1.9 |

[a] Na: ICP; K, Rb and Cs: XRF. [b] Percentage of *M* incorporated in the solid upon the alkaline treatment. [c] volume adsorbed at $p/p_0 = 0.99$. [d] t-plot method. [e] BET method. [f] integrated area of the $CO_2$-TPD profiles. [g] Ratio between the integrated area of the $CO_2$-TPD curves and the alkali metal content expressed as M/(M+Si).

loaded with 0.2 g of catalyst (particle size = 0.2-0.4 mm) and heated at 623 K under a 200 $cm^3\ min^{-1}$ $N_2$ flow. Thereafter, EtOH (0-5% on mole basis) and oxygen (0-3.33 vol.%) were fed keeping a total flow rate of 200 $cm^3\ min^{-1}$. In one type of experiment, the temperature was hold constant for 2 h and then step-wise increased by 50 K with a ramp rate of 5 K $min^{-1}$ from 623 until 773 K. In another kind of test, the catalyst was kept at 723 K for 24 h under a flow of composition 5 vol.% EtOH/2.5 vol.% $O_2/N_2$. The concentrations of EtOH, acetaldehyde (AA) and ethylene in the outlet gas were calculated based on the average of the areas of their respective peaks in four chromatograms acquired every 15 min. Calibration curves were measured in the 0-7 vol.% range for using EtOH (Figure S1 in the ESI, Sigma-Aldrich, >99.5%), AA (Sigma-Aldrich, >99.5%) and ethylene (PanGas, 99.9%). The conversion ($X_{EtOH}$) and selectivity to the product *k* ($S_k$) were calculated as:

$$X_{EtOH} = 1 - (n_{EtOH,1} / n_{EtOH,0})$$

$$S_k = f\, n_{k,1} / (n_{EtOH,0} - n_{EtOH,1})$$

where *n* refers to the moles of EtOH or *k*, 0/1 to the reactor inlet/outlet and *f* is 1 for $C_2$ and 2 for $C_4$ products. The carbon balance was determined as the ratio between the moles of carbon in the gas products and the moles of carbon fed.

## Results and discussion

### Catalyst synthesis and characterisation

**Compositional, porous and structural properties.** A series of post synthetically-modified, high-silica USY zeolites was prepared by alkaline treatment in methanol of a commercial sample featuring a molar Si/Al ratio of 405. The effect of two treatment variables on the properties of the final solids was investigated, *i.e.*, the nature of the alkali metal hydroxide and its concentration. With respect to the first aspect, sodium, potassium, rubidium and caesium hydroxides were selected and applied with the same concentration (0.1 M). The yield of the treatment decreased from 84 to 77% upon increasing the atomic number of the metal cation in the base (Table 1), in agreement with the augmenting basicity of the hydroxide and the consequently higher hydrolytic activity. In line with this, significant amorphisation of the zeolite framework was observed upon use of the stronger bases (Figure 1a, up to 36% loss in crystallinity), which was accompanied by a decrease in micropore volume (Table 1). Interestingly, as previously observed, the methanol-mediated alkaline treatment generated zeolites with inferior mesoporosity compared to the parent material, in contrast to what found for a range of

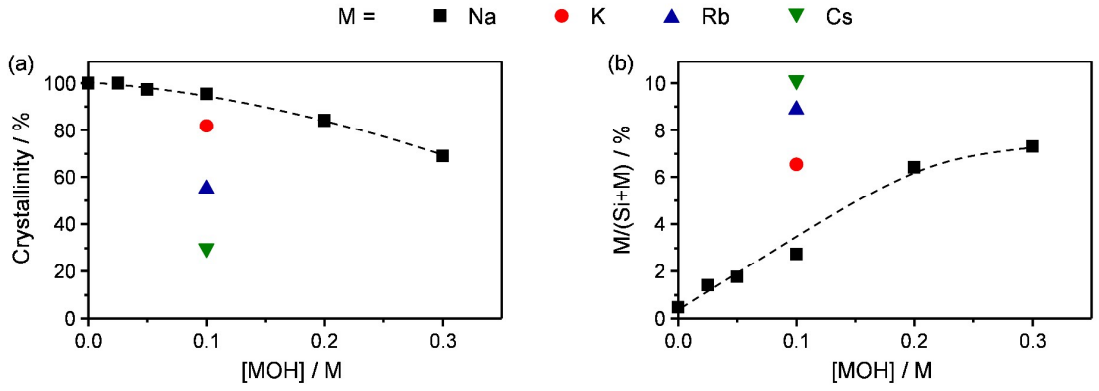


**Figure 1.** (a) Crystallinity and (b) amount of metal incorporated in the USY zeolite upon treatment with alkali metal hydroxide solutions of different concentration.

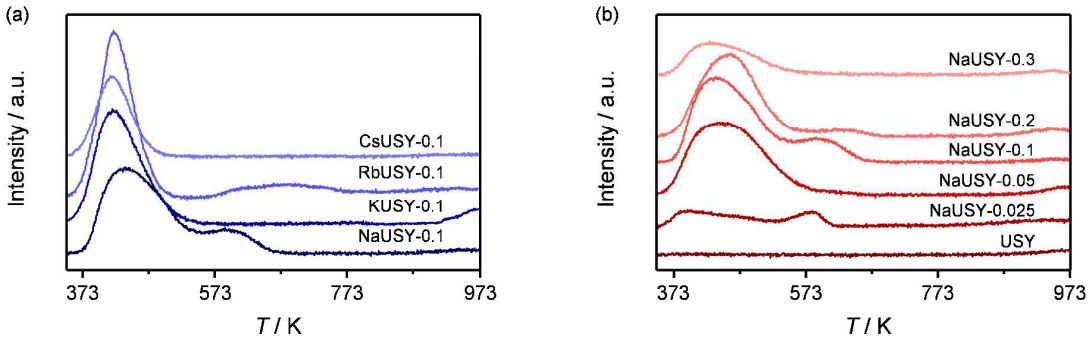


**Figure 2.** $CO_2$ ($m/z = 44$) signal during the $CO_2$-TPD of USY zeolites obtained by alkaline treatment in the presence of (a) hydroxides of different alkali metals and (b) sodium hydroxide solutions of variable concentration.

zeolites upon similar aqueous treatments.[18] The alkali metal content in the final solid (Figure 1b) increased with the atomic number of the cation from 1 to 10 at.%, suggesting that protons of progressively lower acid strength were exchanged in the catalyst. In the case of sodium hydroxide, the variation of the concentration of the methanol solution from 0.025 to 0.3 M resulted in a progressively greater loss of material and crystallinity (Table 1). Additionally, also in this case, the mesopore surface diminished notably. The amount of sodium incorporated was larger at higher hydroxide concentrations (Figure 1b), but the metal incorporation efficiency decreased from 31 to 13%. In this regard, we speculate that the strongest acid protons (*e.g.*, those associated with Brønsted sites) are exchanged more easily, while those at silanol groups of variable but low strength are not exchanged under milder conditions.

**Basic properties.** The basic properties of the prepared materials were investigated by $CO_2$-TPD. In agreement with the higher metal loading (Figure 2a and Table 1), a greater amount of basic sites was detected for the zeolites containing larger metal cations. Nevertheless, their amount relative to the metal content decreased spanning from sodium to caesium. This possibly originates from a higher abundance of alkali metal-bearing siloxy groups at inaccessible positions within the amorphous portions of the materials or from a reduced metal dispersion due to the formation of clustered species.[16,17] The $CO_2$-desorption curves comprised different features depending on the type of metal incorporated in the catalysts. The Na-

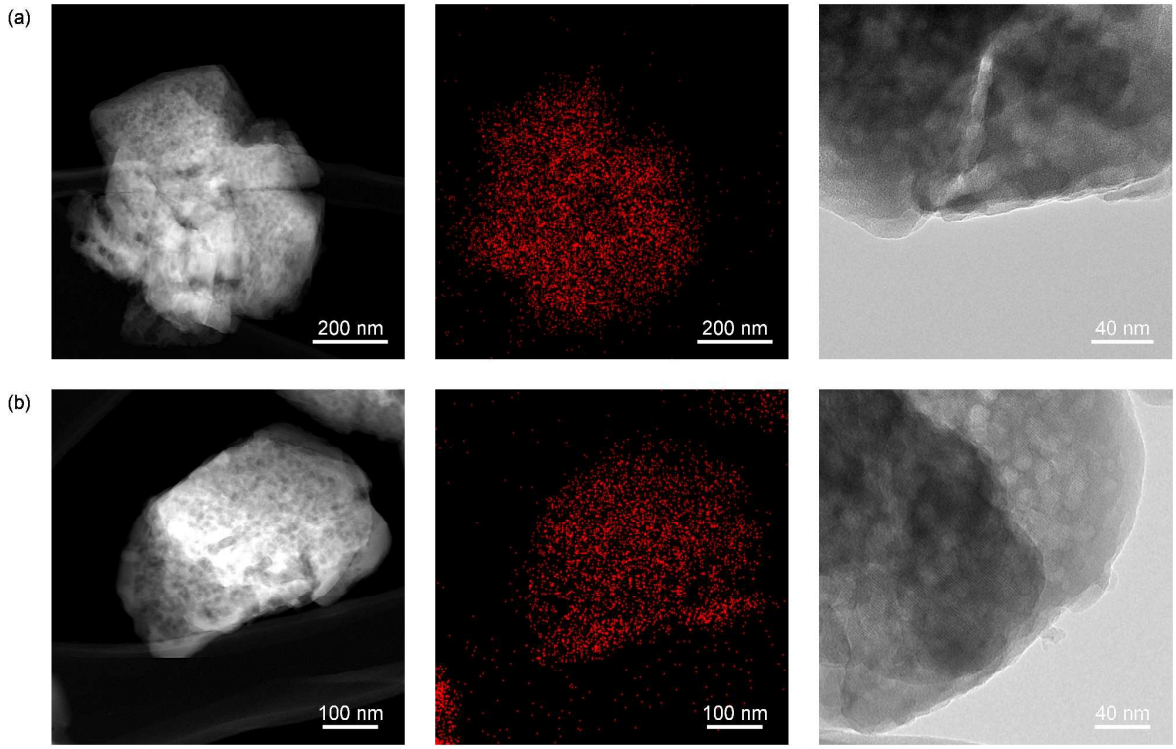


**Figure 3.** HAADF-STEM images, EDS mapping of Na and TEM images (from left to right) of the NaUSY-0.1 catalyst in (a) fresh and (b) used form.

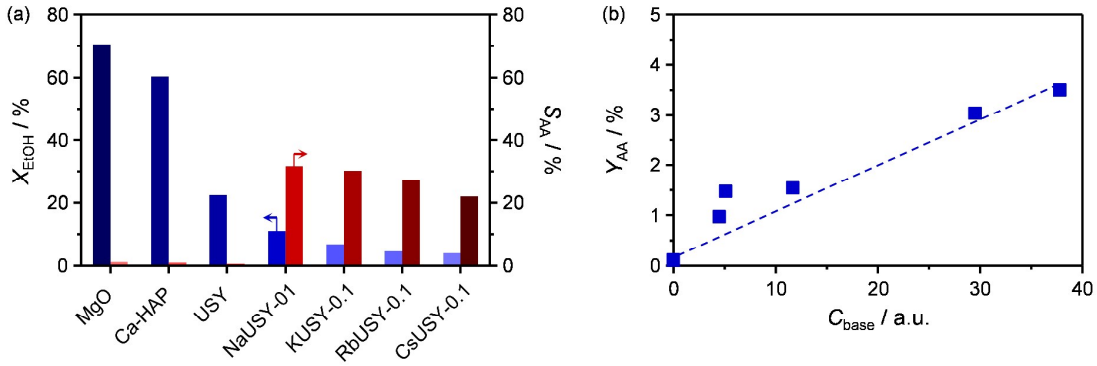


**Figure 4.** (a) EtOH conversion and AA selectivity over state-of-the-art materials and USY zeolite treated in hydroxide solutions of different alkali metals; (b) AA yield over zeolites featuring variable sodium content.

containing material exhibited two main signals between 373 and 673 K, while the profiles of the other samples were dominated by a single signal at 373-520 K. Both the nature of the alkali metal and the distinct amorphisation degree of the zeolite are plausible reasons for the different strength of the basic sites present.

When sodium hydroxide was used at rising concentrations, the basic sites augmented in number (Figure 2b) and the maxima of the low-temperature desorption peak shifted to higher temperature, indicating the formation of stronger basic sites. This is in line with the assumption that weaker acid sites, possibly silanols, were exchanged to their sodium form under harsher conditions. Nevertheless, also in this case, the relative amount of basic sites was lower for the sample containing a higher amount of the alkali metal. Based on the characterisation data of these materials (Figure 1a and Table 1), we put forward the same explanations for this evidence as mentioned above when comparing zeolites with different alkali metals. EDS mapping of Na (Figure 3a) for the sample showing the highest concentration of basic sites relative to the alkali metal incorporated (NaUSY-0.1) evidenced a homogeneous distribution of the alkali metal throughout the particles, indicating a high dispersion of the basic sites. The acidity of the USY zeolite before and after the post-synthetic treatment was probed by FTIR spectroscopy of adsorbed pyridine (Table S1 in the ESI). The parent sample displayed no Brønsted-acid sites and a moderate Lewis acidity, attributed to the traces of aluminum present in the material. No residual acidity was observed on the NaUSY-01 catalyst recovered after

**Table 2.** EtOH conversion and selectivity data for the USY catalysts.

| Catalyst | $O_2$/EtOH (-) | $X_{EtOH}$ (%) | $S_{AA}$ (%) | $S_{ethylene}$ (%) | $S_{C4}$ [a] (%) | $CB$ [b] (%) |
|---|---|---|---|---|---|---|
| MgO | 0 | 88.0 | 1.4 | 31.1 | 44.1 | 79.4 |
| Ca-HAP | 0 | 75.6 | 1.1 | 42.6 | 40.9 | 88.3 |
| USY | 0 | 28.2 | 0.7 | 99.7 | 0.7 | 100.3 |
| NaUSY-0.1 | 0 | 14.1 | 39.4 | 55.4 | 1.4 | 99.5 |
| NaUSY-0.1 | 0.5 | 70.5 | 73.3 | 21.3 | 1.8 | 97.5 |
| KUSY-0.1 | 0 | 7.9 | 37.8 | 61.2 | 5.1 | 100.3 |
| RbUSY-0.1 | 0 | 6.4 | 34.0 | 58.6 | 4.0 | 99.8 |
| CsUSY-0.1 | 0 | 4.9 | 27.4 | 61.1 | 6.9 | 99.8 |

[a] $C_4$ includes ethyl acetate and diethylether. [b] CB: carbon balance.

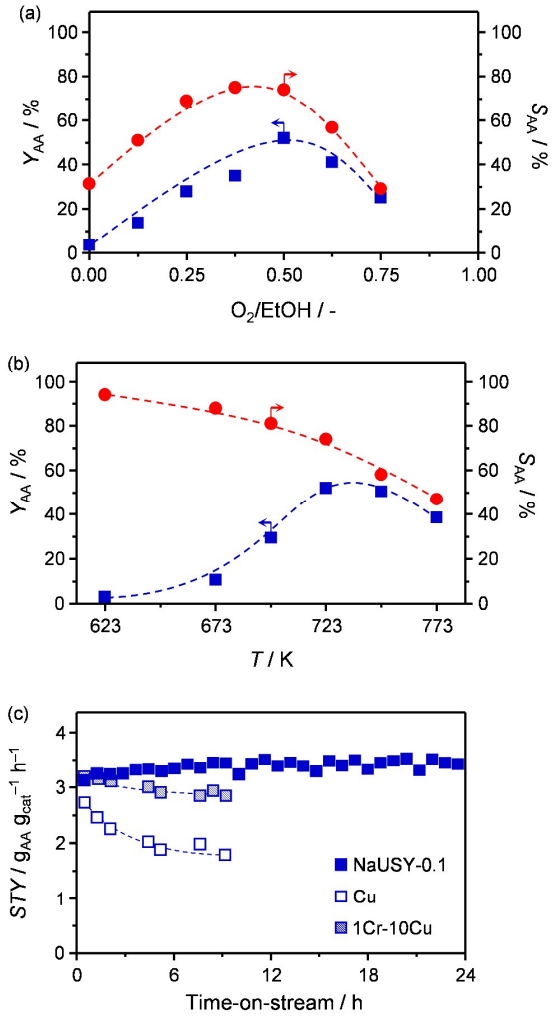


**Figure 5.** Dependence of the yield and selectivity of AA on (a) the $O_2$/EtOH ratio and (b) the temperature. (c) Evolution of the space-time-yield in a 24-h test. Data for the Cu-based systems were retrieved from Ref. 9b.

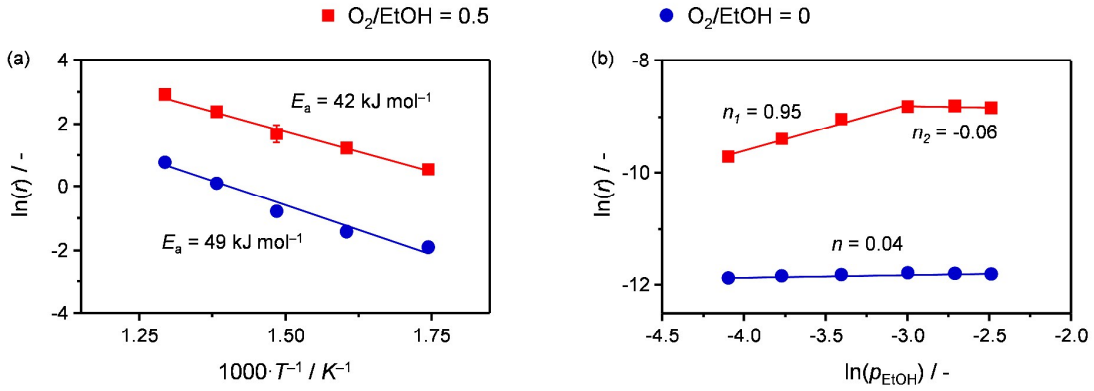


**Figure 6.** (a) Arrhenius plot and (b) dependence of the rate on the partial pressure of ethanol for the NaUSY-0.1 catalyst.

the alkaline treatment.

Conventional basic solids such as MgO and Ca-HAP were also characterised with respect to their acid and basic properties as they were tested as reference in the reaction. Their $CO_2$-TPD curves (Figure S2 in the ESI) evidenced a desorption peak located at higher temperature than for the zeolites, indicating a stronger basic character. No acid sites were detected by FTIR spectroscopy of adsorbed pyridine except for Ca-HAP which exhibited very mild Lewis acidity (Table S1 in the ESI).

### Catalytic evaluation

**Alkali-modified USY zeolites.** The alkali-containing zeolites prepared were tested in the continuous-flow, gas-phase conversion of ethanol into acetaldehyde at 723 K along with the parent zeolite and MgO and Ca-HAP. The starting USY zeolite (Figure 4a) was quite active but displayed a negligible selectivity to the desired product because it mainly produced ethylene *via* dehydration (Table 2), likely due to its Lewis acidity. MgO and Ca-HAP showed a high conversion level but a similarly poor selectivity. Besides for ethylene, they generated a large fraction of $C_4$ species with higher boiling point (Table 2) through condensation. This is consistent with their application in aldol condensations and Guerbet reactions.[19] The post-synthetically modified zeolites containing the various alkali metals displayed an only moderate activity but their selectivity to acetaldehyde was significantly higher. This is in line with their lower acidity. The conversion level was the highest for the Na-containing sample (10%) and progressively decreased in the presence of the larger cations (down to 5%). The selectivity to acetaldehyde followed the same trend being comprised between 39 and 27%.

Overall, it appears that the basic sites of our zeolites are better suited to transform ethanol into acetaldehyde without further conversion through side reactions. Their ability to kinetically favour the dehydrogenation with respect to the dehydration reaction is evident considering equilibrium data calculated in Aspen, which point to an AA selectivity of only 10% under the reaction conditions investigated (Figure S3a in the ESI). Based on the characterisation by $CO_2$-TPD, it is likely that the superiority of NaUSY-0.1 among the alkaline-treated samples is due to the stronger basic sites featured by this material. Its better performance was the reason to prepare distinct catalysts varying the strength of the NaOH solution to verify if further improvement can be attained. Indeed, the properties of alkali-activated zeolites obtained from alkaline methanolic solutions for aldol condensation have been shown to depend on this synthetic parameter.[17] In particular, distinct amounts of basic sites of variable strength and changes in crystallinity were produced applying more or less diluted basic media. As depicted in Figure 4b, a linear correlation was found between

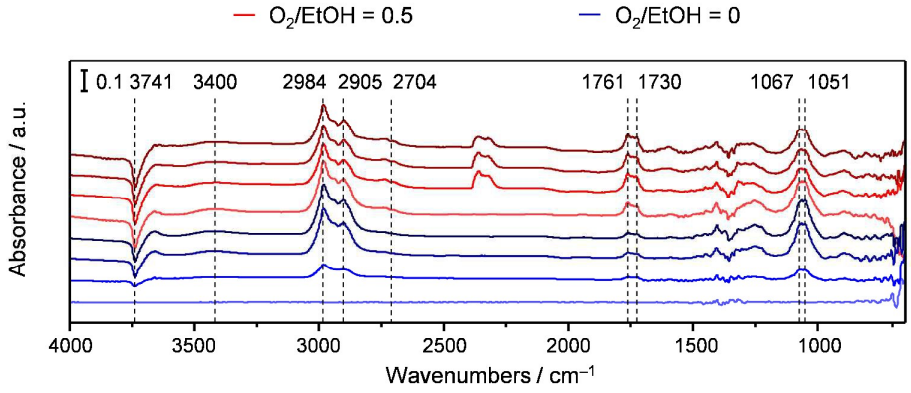


**Figure 7.** *In situ* DRIFT spectra acquired every 5 min (bottom to top) upon ethanol dehydrogenation over NaUSY-0.1 under inert (blue) and oxidising (red) conditions.

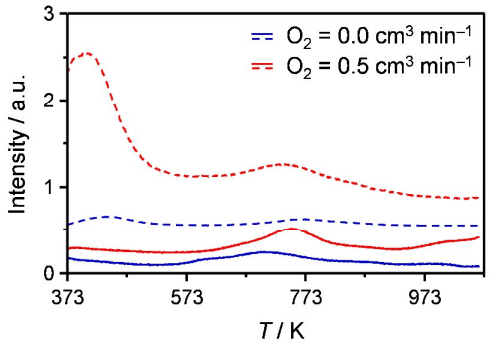


**Figure 8.** Water ($m/z$ = 18, dashed line) and AA ($m/z$ = 44, solid line) signals in the EtOH-TPSR over NaUSY-0.1 in the presence and absence of oxygen.

the acetaldehyde yield and the amount of basic sites in the zeolites. NaUSY-0.1 remained unsurpassed due to its optimal balance between the amount of sodium incorporated and the retention of crystallinity.

**Optimisation of the reaction conditions.** In order to further boost the catalytic performance of this catalyst, we explored the effect of varying operational parameters. At first, we added oxygen to the gas stream as this oxidising agent could assist the dehydrogenation of the reactant. In fact, although the dehydrogenation of ethanol carried out in inert atmosphere, leading to acetaldehyde and molecular hydrogen, is not limited by the thermodynamic equilibrium (Figure S3b in the ESI), the hydrogen abstracted from the alcohol by the basic sites might hinder the adsorption of a second molecule of alcohol if not recombined with another hydrogen atom and evolved from the active centre. Both the acetaldehyde yield and selectivity (Figure 5a) increased up to *ca.* 47 and 75%, respectively, when reaching the $O_2$/EtOH stoichiometric ratio. Thereafter, a decrease was observed which was attributed to the enhanced formation of the total oxidation product $CO_2$. The rate of production of ethylene remained unaffected by the addition of oxygen and was constant over the gas compositions screened. Thereafter, the dependence of the reaction on the temperature was studied at the stoichiometric $O_2$/EtOH ratio (Figure 5b). Also in this case a volcano-shaped curve was observed for the acetaldehyde yield. At low temperature, the very scarce yield was determined by the overall poor activity of the material, while at high temperature, the decline of the yield was due to the greater generation of ethylene and $CO_2$. Testing of NaUSY-0.1 in a 24-h run (Figure 5c) at the optimal $O_2$/EtOH ratio and temperature evidenced outstanding stability, which, remarkably, increased with time on stream because of augmented selectivity. Since 2.3 wt.% carbon was detected in the used material, the latter evidence is likely due to the blocking of unselective sites by fouling. Other deactivation mechanisms, *e.g.*, amorphisation or metal redistribution, could be excluded based on the unaltered structural features and sodium placement evidenced by the microscopic analyses (Figure 3). The robustness of this system largely surpasses that of (promoted) copper-based catalysts,[9b] and, together with the low cost, makes them appealing for a future implementation at a large scale.

**Kinetic and spectroscopic studies**

High-silica, alkali-containing materials have been claimed to possess three adsorption sites for alcohols (R-OH): silanols, alkali ions and Si-O-Si bridges present as defects in the structure.[20] The activity of these solids has solely been attributed to the latter centres, which form an adsorbed ethoxide species (Si-O-R) and a silanol group upon interaction with the substrate.[20] It has been speculated that, under inert conditions, a hydride in $\alpha$-position in the ethoxide species is abstracted by the oxygen of a vicinal silanol forming the acetaldehyde product, which then desorbs restoring the catalytic site.[21] The linear dependence of the dehydrogenation activity of our materials with their alkali-induced basicity is in contrast with the proposed nature of the active centre. Furthermore, the increase in the formation rate of the dehydrogenation product with addition of oxygen (Figure 4a), an effect rarely reported upon the use of non-reducible oxides,[22] cannot be explained by this mechanism. Therefore, gaining fundamental understanding of the mechanistic fingerprint of the dehydrogenation reaction is of primary interest. In this respect, the negligible formation of condensation products over the alkali-activated zeolites constitutes a further remarkable point to be elucidated, being these materials reported as active catalysts for aldol condensations. To this aim, we performed kinetic tests and *in situ* infrared spectroscopic studies.

Concerning the former investigations, we derived an Arrhenius plot measuring the reaction rate at variable temperatures in the presence and absence of oxygen (Figure 6a) and calculated the activation energies associated with the two scenarios. The discrepancy in the values (49 and 42 kJ mol$^{-1}$ for oxygen-free and oxygen-assisted dehydrogenation, respectively) suggests a difference in the rate-determining step or in the underlying mechanism. To clarify this point, we determined the reaction order ($n$) with respect to ethanol (Figure 6b). In the absence of oxygen, this resulted zero, suggesting the saturation of the surface with the reactant, the product or an intermediate. Due to the absence of aldol condensation products, we put forward that under inert conditions the surface is covered by ethoxide species and the formation of acetaldehyde is the likely rate-determining step. When oxygen was co-fed, the reaction order for ethanol was positive (*ca.* 1) at low partial pressures and became zero at higher partial pressures. This hints an Eley-Rideal mechanism,[23] *i.e.*, the adsorbed ethoxide reacts with oxygen from the gas-phase, where the oxygen-assisted formation of the product is rate limiting. The fact that different oxygen species enable the removal of the second hydrogen atom under the two operational modes evidently leads to different activations energies.

To corroborate the hypotheses formulated, we conducted *in situ* DRIFT spectroscopic analyses to gain evidence of the species present at the catalyst surface under reaction conditions (Figure 7). When the NaUSY-0.1 zeolite was exposed to ethanol at 723 K in inert atmosphere, a band attributed to the alcohol in the gas phase was observed at 1067 cm$^{-1}$, along with a contribution at lower wavenumbers

(1051 $cm^{-1}$). The latter is assigned to a negatively charged C-$O^-$ moiety, *i.e.*, ethoxide, adsorbed at Si-$O^-$ basic sites.[24] These spectral features are accompanied by the corresponding and intense absorptions originating from C-H stretching vibrations at 2984 $cm^{-1}$, for gas-phase ethanol, and at 2941 and 2905 $cm^{-1}$, for the ethoxide.[25] In the O-H stretching region, a negative band centred at 3741 $cm^{-1}$ was observed, indicative of a decrease in the amount of terminal silanols.[26] This is in apparent contrast with the formation of ethoxide species at basic sites and the consequent formation of Si-OH species, which would give rise to increased absorbance in this spectral range. Nevertheless, this points to the fact that residual silanols on the material interact with the ethoxide, stabilising it through hydrogen bonds. This is confirmed by the appearance of a broad band centred at 3400 $cm^{-1}$ attributed to hydrogen bonding silanols. The formation of silanols through ethanol adsorption might be masked by the depletion of the original silanols and/or by their interaction with the ethoxide. In the latter case, they shall contribute to the band at 3400 $cm^{-1}$.[27] In line with the observed formation of acetaldehyde, though in low yields, under inert conditions, contributions relative to the stretching of the aldehydic C-H (at 2736, 2704 $cm^{-1}$) and CO (at 1761, 1744, 1730 $cm^{-1}$) groups were detected in the spectra. Since these bands are in good agreement with those reported for acetaldehyde in the gas phase,[28] the only species adsorbed on the catalysts are ethoxide species. Accordingly, the spectroscopic data support the interpretation of the kinetic studies. Additionally, they point to the easy desorption of acetaldehyde as the reason for the negligible generation of condensation products.

When considering ethanol conversion under oxidising conditions (Figure 7), a few differences are noticeable in the DRIFT spectra. Fewer ethoxide species (band at 1050 $cm^{-1}$) are detected compared to the previous case, implying that more catalytic sites are free. This is in agreement with the observation of a positive reaction order at low ethanol partial pressures. The bands related to the aldehyde are more intense, in line with the higher product yields determined in the presence of oxygen. Additionally, the formation of gaseous $CO_2$ (signals between 2400 and 2250 $cm^{-1}$) was observed, suggesting that the total combustion of ethanol occurred as a side reaction to some extent. Still, the spectroscopic results overall corroborate the removal of the hydride from the adsorbed ethoxide as the rate-determining step also in this scenario.

To gain more insights into the action of oxygen, we performed EtOH-TPSR studies under inert and oxidising conditions. The profiles obtained by mass spectrometry analysis of the effluent gases (Figure 8) indicate that when the EtOH-TPSR was performed in the presence of oxygen acetaldehyde was formed in higher amounts, in line with the catalytic data, as well as at lower temperatures. Additionally, they uncover a pronounced water formation in the temperature range of acetaldehyde production only under the use of the oxygen-containing feed. Since the rate of ethylene formation by dehydration in the catalytic tests was constant in both cases, this confirms the direct participation of oxygen in the second step of the dehydrogenation.

## Conclusions

In this study, we have investigated basic zeolites obtained by treatment of high-silica USY materials in methanolic solutions of alkali-metal hydroxides in the dehydrogenation of ethanol into acetaldehyde. The selectivity of these catalysts to acetaldehyde was greatly superior to that of state-of-the-art basic solids such as MgO and hydroxyapatites, owing to their minimal activity for ethanol dehydration and acetaldehyde condensation reactions, resembling that of noble metal-based systems. The product yield increased using sodium hydroxide as the base in the synthesis and tuning its concentration to maximise the amount of basic centres in the solid while substantially retaining the zeolitic structure. At the best reaction temperature identified, the addition of oxygen to the feed significantly boosted both the selectivity (80%) and the yield (50%) of the process. This intriguing effect was rationalised in mechanistic terms performing kinetic studies, *in situ* DRIFT spectroscopic investigations and analyses by temperature-programmed surface reaction of ethanol. We concluded that the reaction is limited by the removal of the second hydrogen atom from the ethoxide species formed upon adsorption of ethanol on the basic sites but that oxygen from the gas-phase, *i.e.*, according to an Eley-Rideal mechanism, is more effective than that silanol groups in this step. In contrast with the rapid deactivation displayed by noble metal-based catalysts, the optimised system exhibited a stable behaviour in a 24-h test, which endows this novel technology with bright prospects for a future industrial application.

## Acknowledgements

This work was sponsored by the Swiss National Science Foundation (Project Number 200020-159760). Dr. S. Mitchell is acknowledged for the microscopic analyses. Mr. H. T. Luk is thanked for the thermodynamic calculations.

## References

1 (*a*) K. Weissermel and H. J. Arpe, *Industrial Organic Chemistry*, Wiley-VCH Verlag GmbH, Weinheim, 4th edition, 2003; (*b*) M. Tu and R. J. Davis, *J. Catal.*, 2001, **199**, 85.
2 M. Beller, B. Cornils, C. D. Frohning and C. W. Kohlpainter, *J. Mol. Catal. A: Chem.*, 1995, **104**, 17.
3 J. Smidt, W. Hafner, R. Jira, J. Sedlmeier, R. Sieber, R. Rüttinger and H. Kojer, *Angew. Chem.*, 1959, **5**, 176.
4 J. J. Bozell and G. R. Petersen, *Green Chem.*, 2010, **12**, 539.
5 (*a*) W.-H. Lin and H.-F. Chang, *Catal. Today*, 2004, **97**, 181; (*b*) H. Amandusson, L.-G. Ekedahl and H. Dannetun, *J. Catal.*, 2000, **195**, 376.
6 (*a*) Y. Q. Liang, Z. D. Cui, S. L. Zhu, Y. Liu and X. J. Yang, *J. Catal.*, 2011, **278**, 276; (*b*) V. L. Sushkevich, I. I. Ivanova and E. Taarning, *ChemCatChem*, 2013, **5**, 2367; (*c*) M. Eckert, G. Fleischmann, R. Jira, H. M. Bolt and K. Golka, *Ullmann's Encyclopedia of Industrial Chemistry*, Wiley-VCH Verlag GmbH, Weinheim, 2014.



 

7 S. P. Tonner, D. L. Trimm, M. S. Wainwright and N. W. Cant, *Ind. Eng. Chem. Prod. Res. Dev.*, 1984, **23**, 384.
8 Y. Guan and E. J. M. Hensen, *Appl. Catal., A*, 2009, **361**, 49.
9 (*a*) Y.-J. Tu, Y.-W. Chen and C. Li, *J. Mol. Catal.*, 1994, **89**, 179; (*b*) Y.-J. Tu, C. Li and Y.-W. Chen, *J. Chem. Technol. Biotechnol.*, 1994, **59**, 141.
10 H. Zhou, J. Y. Wang, X. Chen, C.-L. O'Young and S. L. Sui, *Microporous Mesoporous Mater.*, 1998, **21**, 315.
11 (*a*) M. J. Climent, A. Corma, S. Iborra and A. Velty, *J. Mol. Catal. A: Chem.*, 2002, **182**, 327; (*b*) A. Corma and S. Iborra, *Adv. Catal.*, 2006, **49**, 239; (c) M. Hunger, *Zeolites and Catalysis, Synthesis, Reactions and applications*, ed. J. Čejka, A. Corma and S. Zones, Wiley-VCH Verlag GmbH, Weinheim, 2010.
12 N. Takezawa, C. Hanamaki and H. Kobayashi, *J. Catal.*, 1975, **38**, 101.
13 (*a*) S. Kvisle, A. Aguero and R. P. A. Sneeden, *Appl. Catal.*, 1988, **43**, 117; (*b*) E. V. Makshina, W. Jahnssens, B. F. Sels and P. A. Jacobs, *Catal. Today*, 2012, **198**, 338.
14 Y. Matsumura, K. Hashimoto and S. Yoshida, *J. Catal.*, 1990, **122**, 352.
15 T. C. Keller, S. Isabettini, D. Verboekend, E. G. Rodrigues and J. Pérez-Ramírez, *Chem. Sci.*, 2014, **5**, 677.
16 T. C. Keller, E. G. Rodrigues and J. Pérez-Ramírez, *ChemSusChem,* 2014, **7**, 1729.
17 T. C. Keller, K. Desai, S. Mitchell and J. Pérez-Ramírez, *ACS Catal*., 2015, **5**, 734.
18 D. Verboekend, G. Vilé and J. Pérez-Ramírez, *Adv. Funct. Mater.*, 2012, **22**, 916.
19 (*a*) J. I. Di Cosimo, V. K. Díez and C. R. Apesteguía, *Appl. Catal., A*, 1996, **137**, 149; (*b*) W. Ueda, T. Kuwabara, T. Ohshida and Y. Morikawa, *J. Chem. Soc., Chem. Commun.*, 1990, 1558.
20 Y. Matsumura, K. Hashimoto and S. Yoshida, J. *Catal.*, 1991, **131**, 226.
21 (*a*) Y. Matsumura, K. Hashimoto and S. Yoshida, *J. Mol. Catal.*, 1991, **68**, 73; (*b*) G. Larsen, E. Lotero, M. Márquez and H. Silva, *J. Catal.*, 1995, **157**, 645.
22 S. Yao, F. O. Yang, S. Shimumora, H. Sakurai, K. Tabata and E. Suzuki, *Appl. Catal., A*, 2000, **198**, 43.
23 D. D. Eley and E. K. Rideal, *Nature*, 1940, **146**, 401.
24 (*a*) T. W. Birky, J. T. Kozlowski, R. J. Davis, *J. Catal.*, 2013, **198**, 130; (*b*) K. Chandran, R. Nithya, K. Sankaran, A. Gopalan and V. Ganesan, *Bull. Mater. Sci.*, 2006, **29**, 173.
25 C. P. Bezoukhanova and Y. A. Kalvachev, *Catal. Rev. -Sci. Eng*., 1994, **36**, 125.
26 G. Larsen, E. Lotero, M. Márquez and H. Silva, *J. Catal.*, 1995, **157**, 645.
27 L. Kubelková, J. Čejka and J. Nováková, *Zeolites*, 1991, **11**, 48.
28 J. C. Evans and H. J. Bernstein, *Can. J. Chem*., 1956, **34**, 1083.

# Table of Contents graphic

## Selective dehydrogenation of bioethanol to acetaldehyde over basic USY zeolites

Giacomo M. Lari, Kartikeya Desai, Cecilia Mondelli and Javier Pérez-Ramírez*

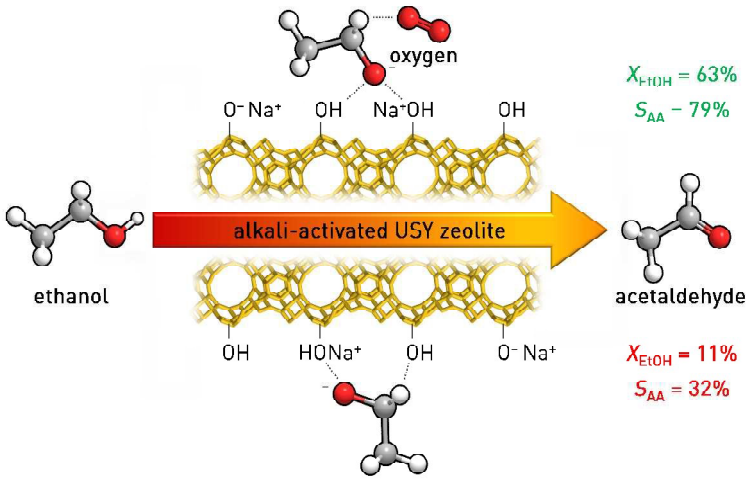


Alkali-activated zeolites are active, selective and stable catalysts for ethanol dehydrogenation to acetaldehyde. Molecular oxygen eases hydrogen abstraction from the adsorbed ethoxide intermediate boosting the catalytic performance.